Indoor heterogeneous photochemistry of furfural drives emissions of nitrous acid

A. Depoorter, C. Kalalian, C. Emmelin, C. Lorentz, C. George

Indoor heterogeneous photochemistry of furfural drives emissions of nitrous acid

A. Depoorter[†], C. Kalalian [†], C. Emmelin[†], C. Lorentz[†], C. George[†]

† Univ Lyon, Université Claude Bernard Lyon 1, CNRS, IRCELYON, F-69626, Villeurbanne, France.

Abstract

People spend approximately 80% of their time indoor, making the understanding of the indoor chemistry an important task for safety. The high surface-area-to-volume ratio characteristic of indoor environments leads the semi-volatile organic compounds (sVOCs) to deposit on the surfaces. Using a long path absorption photometer (LOPAP), this work investigates the formation of nitrous acid (HONO) through the photochemistry of adsorbed nitrate anions and its enhancement by the presence of furfural. Using a high-resolution proton transfer reaction-time of flight-mass spectrometer (PTR-TOF-MS), this work also investigates the surface emissions of VOCs from irradiated films of furfural and a mix of furfural and nitrate anions. Among the emitted VOCs, 2(5H)-furanone/2-Butenedial was observed at high concentrations, leading to maleic anhydride formation after UV irradiation. Moreover, the addition of potassium nitrate to the film formed NO_x and HONO concentrations up to 10 ppb, which scales to ca. 4 ppb for realistic indoor conditions. This work helps to understand the high levels of HONO and NO_x measured indoors.

Keywords

Indoor air quality, Furfural, Nitrous Acid, Surface reaction, Photochemistry

Practical implications

Furfural is a ubiquitous pollutant indoors, which in the adsorbed state, induces photochemical properties to indoor surfaces. This photochemistry is shown here to significantly enhance the formation of nitrous acid and therefore impact the oxidation capacity indoors.

1. Introduction

Current atmospheric chemistry knowledge, built over the last decades, was found to be insufficient when applied to indoor air chemistry[1]. The indoor environment is a complex mix of sources and sinks due to biogenic, human and microbial activities under unique conditions (e.g., light, humidity and temperature)[2,3]. For instance, volatile organic compounds (VOCs) are often present in higher concentrations indoors than outside, affecting its air quality[4–7]. Furfural is a VOC emitted from multiple materials, generally produced under thermal stress from the degradation of polyoses (hemicelluloses)[3,8,9] through a mechanism previously described[10]. Furfural is expected to be present indoor, emitted from surfaces of wood based products[11] which are known to be an important source of indoor pollutants[12]. Concentrations measured in Italy and Finland reveal average levels of few µg m^{-3} with levels reaching up to 39 µg m^{-3} [9,13,14] in homes, offices and public buildings, and was observed in dust in houses at about 20 µg g^{-1} [15] in Sweden. Recently, experiments were conducted within the House Observations of Microbial and Environmental Chemistry, aiming to understand the indoor chemistry in the average US home. Average indoor concentration measured were similar to the concentrations observed in Europe at about 4 µg m^{-3} and decreased by a factor 10 when the room was ventilated. The presence of furfural at comparable levels in Europe and the US highlights its importance independently of the architectural styles i.e., it is not limited to wooden houses. It was determined that the time required for the furfural to reach steady state concentration indoor is shorter than the average air renewable rate, indicating that surfaces act as an important reservoir of this VOC[11]. As high concentrations measured in some buildings can be linked to the presence of books and wooden furniture[9,14], incense burning is also a major source of furfural leading to harmful concentrations of the order of magnitude of 10^1 mg m^{-3} [16]. The occupational exposure limit was set to 8 mg m^{-3} over a period of 8 hours[17]. Furfural is regarded as a key product in the chemical industries, hence its production was deeply researched in the 20th century[18]. It

currently has many uses in the industry as a solvent. It could also be used as a marker for indoor air quality control due to his abundance and volatility [19].

Indoor surfaces are a medium where a wide range of compounds can react, offering a complex chemistry that can be affected by indoor light. While volatile compounds are rapidly ventilated out in most indoor environments, semi-volatile compounds (sVOCs) tend to adsorb on surfaces due to the high surface-area-to-volume ratios (ranging from 1 to 2 m^2 m^{-3})[20,21], and are therefore sustained for longer times. It is acknowledged that ozone indoor is lost primarily through reactions on the surface leading to the formation of VOCs[22]. Other gas phase compounds can react on the surface such as NO_2 through hydrolysis[23] as well as HONO that can interact with indoor surfaces to produce hazardous compounds like nitrosamines[24]. In additions, nitric acid can be photolyzed when organic coating are present on the surface[25].. Surfaces with specific coatings such as paintings could also produce organic indoor air pollutants like VOCs, NO_x and HONO when exposed to UV irradiation[26–29]. While indoor irradiation is less intense than outside and high energy wavelengths below 330 nm are scarce, photochemistry is still an important factor indoors[30–34].

The hydroxyl radical ($OH^{\cdot}$) was found to be a major indoor oxidant, which was thought to be mainly produced from the ozonolysis of unsaturated VOCs[35]. However, a recent study by Mendez et al.[21] showed that the photolysis of nitrous acid (HONO) can also be a significant source of OH radicals, contributing to more than 50% of their sources[31,36]. HONO can be produced heterogeneously through the processing of adsorbed nitrate anions or gaseous nitrogen oxides, which are ubiquitous indoors[32,37]. Arata et. al.[38] recently reported direct measurements of indoor N_2O_5 and NO_3, which can participate in reactions producing HNO_3. Indoor nitric acid is not readily photolyzed and is likely to deposit onto surfaces, where water layers could lead to hydrolysis and production of surface nitrate. Nitrate was measured on indoor surfaces with concentrations varying from 10^{-3} to 10^{-5} mol m^{-2} [39,40].

In this paper, the photochemistry of deposited furfural and its implication in converting nitrogen oxides or adsorbed nitrate anions into gaseous HONO and NO_X were investigated through laboratory experiments. Furfural seems to be a ubiquitous VOC emitted from surfaces[9,11,13,14], and here we suggest that its presence on these surfaces is conferring photosensitizing properties to them. Those properties are tested here by investigating the photoconversion of adsorbed nitrate to HONO, and the formation of surface peroxy radicals. This knowledge will lead to a better description of surface photochemistry indoors, and possibly closing a gap in our understanding of indoor HONO and hydroxyl radical formation.

2. Materials and Methods

As stated above, our aim is to explore the photosensitizing properties of adsorbed furfural representative of indoor wooden surfaces. We therefore prepared and exposed organic films made of deposited furfural, doped or not with nitrate anions, to light emitted from a LED in a small photo reactor described below. Gaseous products, including VOCs and HONO were monitored, and the production of surface peroxy radicals probed indirectly by their titration with NO.

2.1. Experimental protocol

2.1.1. Film preparation

Aqueous solutions of furfural and potassium nitrate were prepared in Milli-Q water (18.2 MΩ cm) with concentrations varying from 0.01 M to 0.5 M and 0.01 mM to 1 M, respectively. Two mL of a fresh solution was evenly dispersed on a circular borosilicate glass window (50 mm diameter). The glass window was weighed before the preparation, dried over a period of 12 hours in a desiccator filled with silica gel desiccant and placed in an oven at 323.2 ± 0.1 K. Once dried, the glass windows were weighed again and used in an experiment within one day.

2.1.2. Irradiation setup

The organic films deposited on the glass substrates were placed at the bottom of a borosilicate glass reactor (height = 4 cm; volume = 80 cm^3) and irradiated for 45 minutes (or more) using a LED lamp (M340L4; Thorlabs, λ_{max} = 345 nm, nominal maximum irradiance 2.22 W/m^2) placed 2 cm above the reactor. The humidity within the reactor was adjusted by varying the flows of synthetic air or synthetic N_2 passing through a bubbler or connected directly to the reactor.

This reactor was maintained at room temperature and flushed with nitrogen or synthetic air at a flow rate of 90 mL min^{-1}. The outlet of the flow cell was connected to all the analytic devices described above.

For the experiments of NO uptake (section 3.4), a constant gas flow of nitric oxide at [NO] = 68 ± 2 ppb was used. To stabilize the NO concentration, the flow first bypassed the reactor and was then injected into the reactor at the beginning of the film exposure.

2.2. Analytical devices and protocols

2.2.1. UV analysis

The UV-vis absorption of the organic films in the range 200–600 nm by means of Cary 60 UV-Vis spectrophotometer (Agilent Technologies) in the liquid (after extraction) and solid (adsorbed) phases. The solid-liquid extraction was performed by rinsing the films with 2 mL of Milli-Q water. This solution which was then diluted between 2 and 20 times prior to be optically probed in 3500 µL Macro Fluorescence Cuvette (Thorlabs). The absorption of the solid films was simply probed by placing the circular borosilicate glass window on which the organic film was adsorbed perpendicularly to the optical beam within the spectrometer. Each analysis was performed on three different locations of the film and then averaged, and the absorbance from the glass window subtracted.

2.2.2. PTR-TOF-MS analysis

In order to monitor the emissions of volatile organic compounds (VOC) from the furfural films, a proton transfer reaction-time of flight mass spectrometer (PTR-TOF-MS, 8000 - Ionicon Analytik GmbH, Innsbruck, Austria) was deployed, as described in detail by Ponczek and George[24]. This soft ionization procedure limits, while not preventing as discussed by Ŝpaněl et al.[25], the fragmentation of the VOC to be analyzed and enables to the detection of a large number of compounds.

All PTR-TOF-MS measurements were performed using the H_3O^+ ionization mode with the following parameters: source current of 4.0 mA, drift tube voltage of 600 V, drift tube temperature of 373 K, inlet temperature at 353 K and a drift pressure of 2.20 mbar. The E/N was about 123 Td. Spectra were collected at a time resolution of 10 s. Mass calibrations were performed using internal calibration based on two ions with known mass: hydronium ion isotope ($H_3{}^{18}O^+$ m/z 21.022) and protonated acetone (C_3H_7O+ m/z 59.049).

2.2.3. High-resolution NMR analysis

Characterization of the furfural films by ^{1}H NMR were carried out using a Bruker AVANCE HD (400 MHz) spectrometer equipped with a 5mm BBFO Z-gradient probe. The films were dissolved in 1 mL DMSO-d6 and 600 µL of this solution was used for the NMR tube preparation. Quantitative ^{1}H NMR was carried out at a frequency of 400.13 MHz using a 30° flip angle (3.1 µs) with a recycle delay of 1 s and an acquisition time of 5 s. Sixteen scans of single pulse ^{1}H excitation were collected over a spectral width of 20 ppm. Data were acquired and processed with Bruker topspin 3.2 software.

2.2.4. HONO and NO_x gaseous analytics

A Long Path Absorption Photometer (LOPAP, QUMA) was used to measure the concentrations of gaseous HONO[23]. In brief, HONO was sampled in a stripping coil by a fast-chemical reaction and converted into an azodye, which was photometrically detected in a long path absorption cell. The inlet gas flow was set to 500 mL min^{-1} and the integrated time resolution was set at 7

152 min with a detection limit less than 10 ppt. The liquid flow used for the reactants was set to 20
153 ml min^{-1} and the sampling unit was maintained at 293 ± 0.02 K using a (Thermo Scientific
154 ARCTIC Refrigerated/Heated Bath SC100 A10 - 230V), which was calibrated each week.
155 A standard chemiluminescence NO_X analyzer (CLD 88 CY analyzer, Eco Physics) was used
156 to monitor NO and NO_2 concentrations, with a detection limit of 50 ppt. In the first channel,
157 NO reacts with O_3 to produce NO_2*, which emits a radiation (λ_{max} = 1200 nm) detected by a
158 photomultiplier. A second canal allows NO_2 to be converted to NO using a reductor agent with
159 a yield of 70%. The NO_2 concentration was obtained by calculating the difference measured
160 between the two channels.

161 ***2.3. Reagents***

162 Furfural (99%), potassium nitrate (≥99.0%) and dimethyl sulfoxide-d_6 (99.9%) were provided
163 by Sigma Aldrich; NO (1 ppm in N_2) was from Linde, synthetic air (>99.9%) was from Air
164 Products and N_2 was synthetic (>99.9992%). The silica gel desiccant used was provided by
165 Alfa Aesar (indicating, ACS, -4 + 10 Meh Granules) and Drying Pearls Orange was from Sigma
166 Aldrich. The glass windows were made of borosilicate except one made of quartz and were
167 used for the UV analyses of the films.
168

169 **3. Results and discussion**

170 ***3.1. Film characterization***

171 During the film preparation, more than 99% of the mass of furfural was lost by evaporation of
172 the product. For instance, after depositing 96.1 mg of furfural from 2 mL of a solution at 0.5
173 M, only 0.7 ± 0.4 mg remained after the drying procedure. In other words, all the experiments
174 were performed on very thin films made only from furfural residues. To characterize these
175 films, UV and ^{1}H NMR analyses were carried out.

176 To understand the influence of the preparation process on the structure of furfural, UV
177 analyses were performed on deposed and extracted films in 2 mL of Milli-Q water and
178 compared to two control solutions of pure furfural solutions at different concentrations (0.01
179 and 0.02 mM) (Figure 1). The control solutions of furfural presents UV absorption bands at 277
180 nm and 228 nm, characteristic of the aldehydic and furan functional groups, respectively. We
181 observed that the UV spectra of films in liquid and solid phases indicated a transformation of
182 the furfural on the surface with light absorption in the visible range (<600 nm) and presented a
183 new band at 340 nm. The intense absorption between 200 and 250 nm indicates the conservation
184 of the furan function while the aldehydic band is shifted, indicating a transformation, which
185 was later confirmed by ^{1}H NMR and PTR-TOF-MS analyses. We hypothesized that the
186 structure of the film could correspond to polymeric structures, as seen in the literature[44,45].
187 Furfural can indeed undergo self-condensation under anhydrous conditions or thermal
188 treatment at 373–523 K[18,44] and could also form humins[46,47]; however, the mechanism is still
189 unclear[46–48]. Such chemical processes result in the formation of polyfurylic structures (Figure
190 2). The band at 340 nm could correspond to maleic anhydride and/or 2-acetylfuran; both of
191 these are products emitted in the gas-phase from furfural films, as discussed in section 3.2.

192 The UV analysis of a furfural film that was irradiated by the LED lamp at 340 nm over
193 time (see Figure S1) showed a change in the shape of the band centered at 340 nm, along the
194 irradiation time, implying a possible degradation of the sample and a chemical transformation
195 of the surface. This change in composition upon irradiation will be important for describing the
196 temporal behavior of HONO emissions discussed in section 3.3.

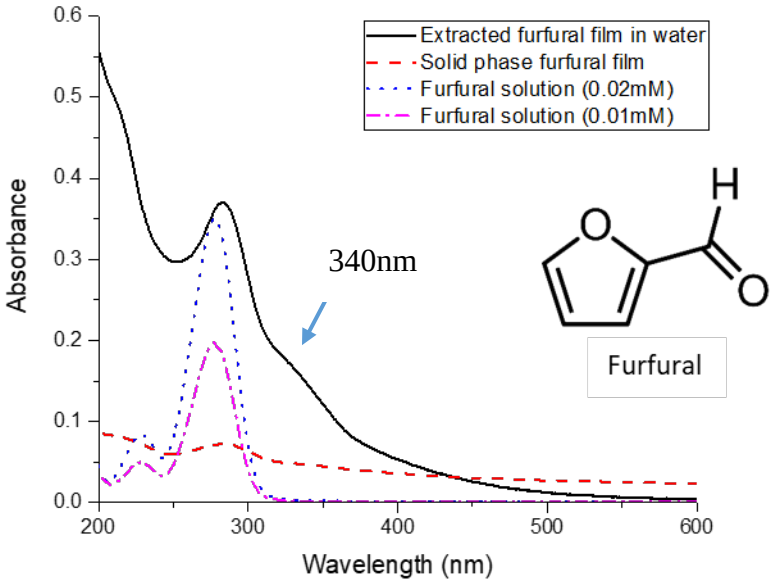

197

198 **Figure 1:** The UV spectra of a furfural-extracted film, a solid film and aqueous solutions of
199 pure furfural (0.01 mM, 0.02 mM). The films were not irradiated.

200

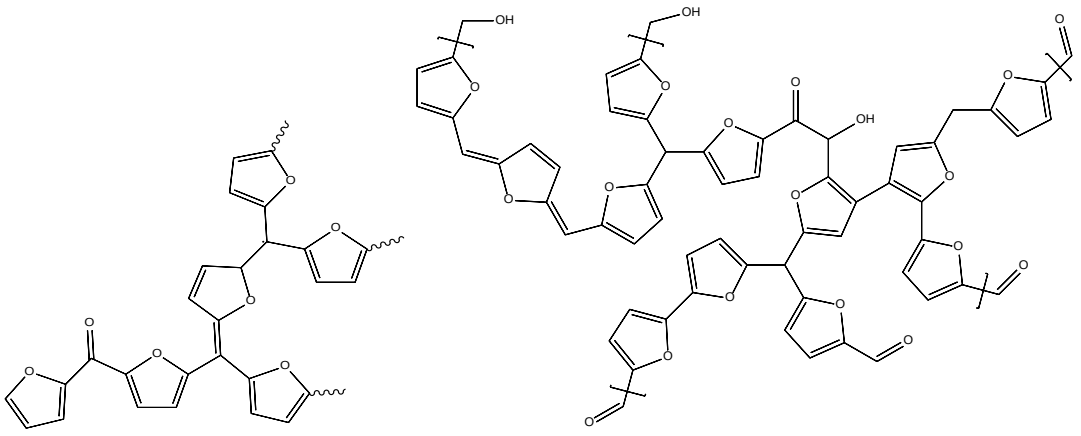

201

202 **Figure 2:** The chemical structure of the suggested polyfurylic oligomer (left)[44] and humins
203 (right)[45]

204

205 Moreover, the ^{1}H NMR analyses showed broad peaks, confirming the complex nature of
206 furfural films[49]. The proton peak from the aldehyde (9.4 ppm) group in furfural was not found,
207 while the other proton signals could not be identified due to the complexity of the spectra

between 6 to 8 ppm (see Figure S2a). An important peak at 6.1 ppm was associated with the presence of an enone group in the structure of the oligomer/humin. The low intensity of the signal at 9.5 ppm is also in agreement with the hypothesized structure of the oligomer without aldehydic or carboxylic groups. When potassium nitrate is added to the film, the spectra changed and new peaks appeared. A peak at 4.9 ppm, absent from samples without potassium nitrate, indicated the presence of nitro groups (see Figure S2b). The presence of these groups involved a reaction between nitrate anions and furfural during the film preparation process. Tests performed on the influence of humidity and irradiation of the film (45 min, with and without nitrate) did not result in a significant modification of the ^{1}H NMR spectra (see SI Figure 2a).

3.2. VOC production

The PTR-TOF-MS analyses were performed on furfural films at two different relative humidities (<1 and 90%) under dark and irradiation conditions without nitrate. When the films were exposed in the dark to dry synthetic air (RH < 1%), no significant VOC formation was observed, however when the humidity was high (RH = 90 ± 1%), numerous VOCs were observed compared to a blank experiment without furfural (see Figure 3 and Table S1). The presence of the 2,5-Furandicarbaldehyde (also known as 2,5-Diformylfuran; mass-to-charge ratio of m/z = 125.03), 2-Acetylfuran or 5-Methylfurfural (m/z = 111.04) and more complex structures involving derivatives of furan (m/z = 123.05 and 139.04) confirms the transformation of furfural during the film preparation, as suggested from the hypothesized oligomeric structures. Some compounds were unsaturated and possibly conjugated including 2,5-Diformylfuran, Furylacrolein, 1-(2-Furyl)-1,2-propanedione, explaining the increase of the maximum of UV absorbance toward visible light, as seen in section 3.1. The presence of enones, as suggested by the ^{1}H NMR analyses, was confirmed by the presence of malondialdehyde, furylacrolein and arolein. The compound emitted from the surface with the

highest relative abundance had a mass-to-charge ratio of *m/z* = 85.02. This ion could be attributed to 2(5H)-furanone, which forms from the furfural oxidation under harsher conditions[50]. It could also correspond to the isomer 2-butenedial; however, its formation during the film preparation is unclear. Under UV irradiation, maleic anhydride (*m/z* = 99.01) was formed at high relative abundance (see Figure S3). Photochemistry of both 2(5H)-furanone and 2-butenedial could explain the formation of maleic anhydride[50–52]. However, only the photochemistry of 2-butenedial is activated at the wavelengths used in this study. Experiments carried with varying concentrations of oxygen in the gas phase have shown that maleic anhydride formation requires the presence of O_2 as described in the mechanism by Newland et al.[51] (see Figure S4). Nineteen compounds were found to be released at higher concentrations when the sample was irradiated (see Table S2). Direct emissions through the scission of small molecules from the suggested structures described in the literature could be the origin of these VOCs[53].

The presence of an organic compound (furfural in this study) modifies the molecular structure of adsorbed nitrate anions, leading to a red-shift in the actinic region and increasing the light absorbed by nitrate anions[54]. Due to the presence of high levels of acids on the surface, nitrate is transformed into nitric acid. Adsorbed nitrate/nitric acid ($HNO_{3(s)}$) photolysis can directly produce HONO and NO_2 following reactions R1 and R2. It can produce HONO indirectly through reactions R3 and R4[54,55] , with $Org_{(s)}$ corresponding to furfural in this study, as follows:

$$HNO_{3(s)} \xrightarrow{h\nu} NO_{2(s)} + OH_{(s)} \quad \text{(R1)}$$

$$HNO_{3(s)} \xrightarrow{h\nu} HONO_{(s)} + O(^3P)_{(s)} \quad \text{(R2)}$$

$$NO_{2(s)} + H_2O_{(s)} \xrightarrow{h\nu} OH_{(s)} + HONO_{(s)} \quad \text{(R3)}$$

$$NO_{2(s)} + Org_{(s)} \xrightarrow{h\nu} Org - oxidized_{(s)} + HONO_{(s)} \quad \text{(R4)}$$

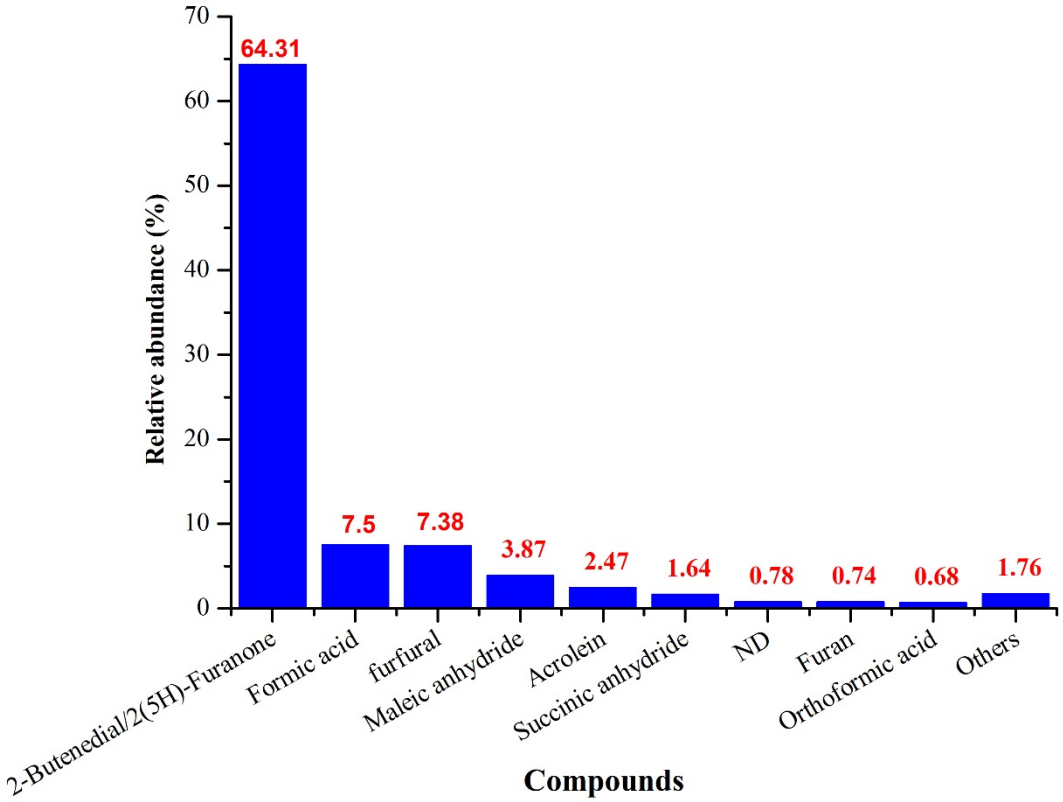

Figure 3: Relative abundance of the most emitted VOCs from furfural films under dark condition and at high relative humidity (90 ± 1%)

The addition of nitrate to the film changed the emission profile of the surface. Concentrations of the products emitted from the film with and without irradiation were enhanced up to a factor of 10 for maleic anhydride and furfural. Concentrations of compounds of higher mass than the furfural were also greatly enhanced; these compounds included succinic/fumaric acid, 2,5-Diformylfuran and 1-(2-Furyl)-1,2-propanedione. Unidentified compounds (*m/z* = 151.05 and 169.05) $C_8H_6O_3$ and $C_8H_8O_4$, respectively, were also found at higher concentrations. The formation of a new compound was also observed at *m/z* = 124.01 and was identified as $C_6H_3O_3$. Experiments with different concentrations of nitrate showed an evolution of VOC concentrations in relation to the quantity of nitrate on the surface. This increase showed that

nitrate interacts with the film and decreases the loss of furfural by evaporation during the sample preparation.

3.3. Addition of nitrate anions – HONO formation

Nitrate photochemistry is unlikely to occur under indoor conditions due to the lack of wavelengths below 330nm. However, a photosensitization pathway could certainly promote its photo conversion to HONO. In this study we explored this possibility on films made of deposited furfural

When potassium nitrate was added to the furfural films, an enhanced production of HONO was observed. It is important to underline that under our conditions, in the absence of furfural, irradiated potassium nitrate on the surface was unable to produce HONO. In fact, the range of wavelengths (335-380 nm) emitted from the LED lamp used in this experiment does not allow the activation of the photochemistry of potassium nitrate. KNO_3 does not absorb significantly after 335nm[56,57].

The amount of HONO produced was dependent on the quantity of furfural deposited, as measured by its initial concentration in the parent solution. An increase in the concentration of furfural from 0.05 to 0.5 M with a concentration of 10^{-1} M of KNO_3 increased the formation of HONO by a factor of 10 (Figure 4a). A similar trend can be measured for the absorbance at 345nm of extracted films in water. However, the deposited nitrate mass had only a slight effect on the formation of HONO from 10^{-4} to 10^{-1} M, which could be expected from a stoichiometric reaction between the furfural oligomer, the nitrate and a stabilization of the furfural present on the surface by the nitrate, as the PTR analyses have shown (Figure 4b). Also, when nitrate is highly concentrated (1 M in the parent solution), the formation of HONO decreases; this is possibly due to the fact that gaseous products formed in the photolysis process may hardly

escape from the nitrate crystal layer formed on the top of the film. This phenomenon was previously observed by Yang et al [58]. The UV analyses of this film showed a broad absorption band from 300 to 600 nm, which can prevent the UV irradiation from reaching the furfural film below the nitrate layer.

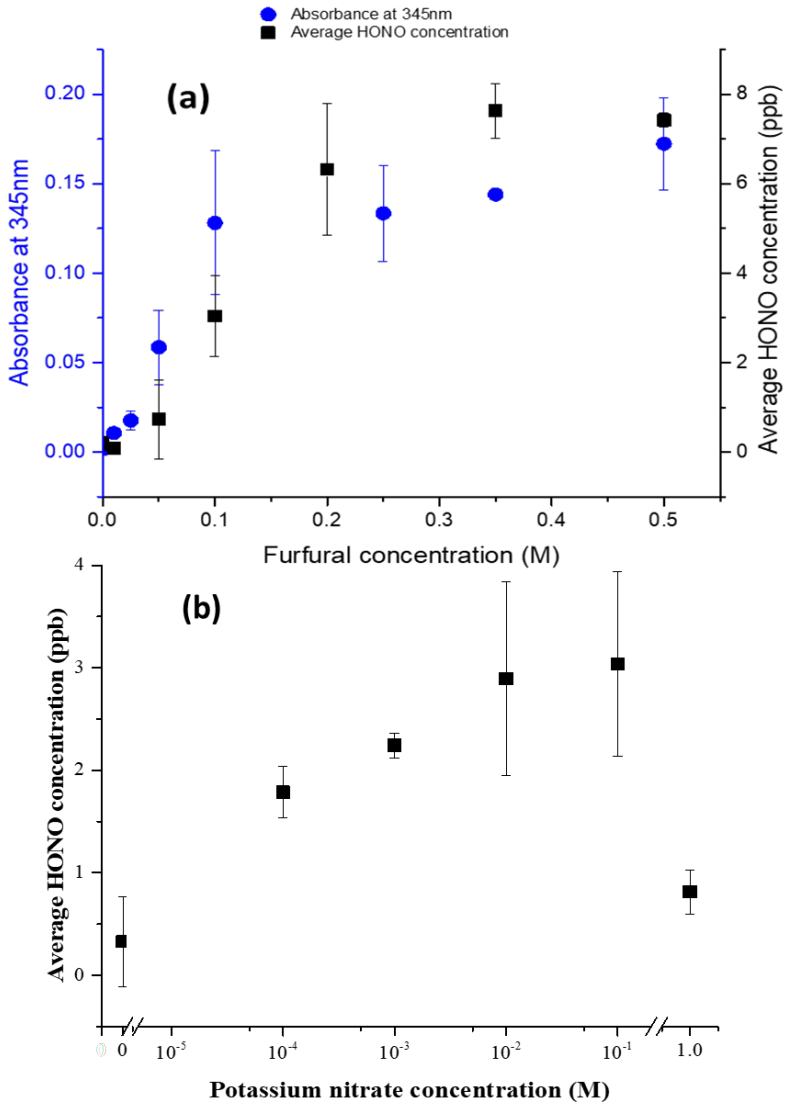

Figure 4*:* (a) Formation of nitrous acid from an irradiated film of furfural + KNO_3 (0.1 M) and the absorbance of the film at 345 nm, as a function of the used furfural concentration. (b) Formation of nitrous acid from an irradiated film of furfural (0.1 M) + KNO_3 as a function of

potassium nitrate concentration. The average HONO concentration was calculated by integrating the signal during the first 45 minutes of irradiation. Errors are ± 2σ.

To explain the photochemical formation of NO, NO_2 and HONO, we propose a mechanism based on our observations and the literature[59–62] (Figure 5). 2-nitrofuran is used as a proxy of the nitro compounds formed in the film and observed during the NMR analyses**.** The degradation of 2-nitrofuran leads to two possible products: $[M+H]^+$ = 84.02 and $[M+H]^+$ = 69.02 corresponds to $C_4H_3O_2$ and C_4H_4O, respectively. Furan is already a product observed when irradiating a film made from furfural only; however, when nitrate is added, the photochemistry is enhanced according to the signals detected during the PTR-TOF-MS analyses. Those products could result from the loss of NO and NO_2 as shown in Figure 5. In addition, NO_2 could be further reduced to HONO on the surface containing reducing functionalities such as soot[63] or humic acids[64,65].

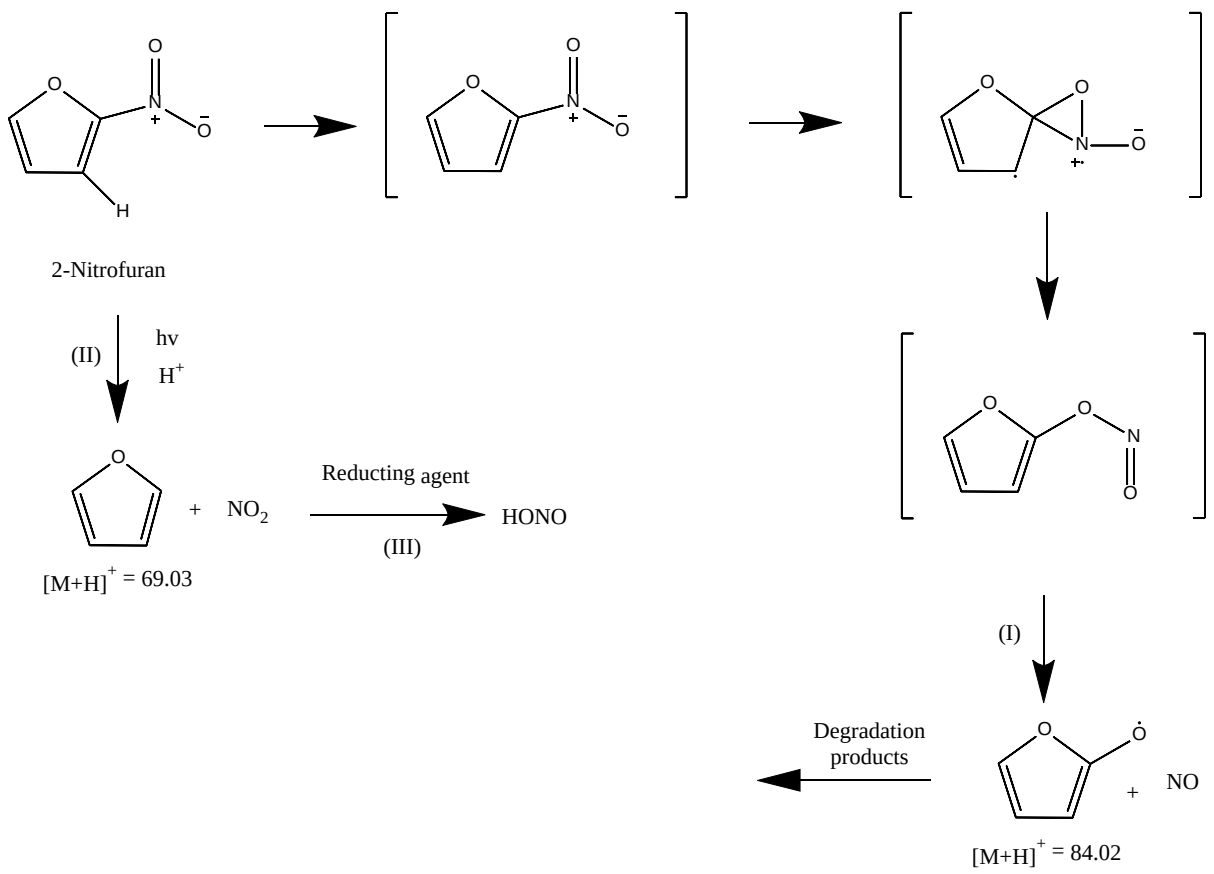

Figure 5: Suggested mechanism of formation of NO, NO_2 and HONO from 2-Nitrofuran under UV irradiation.

This photochemistry was observed under pure nitrogen. The addition of O_2 while maintaining a constant flow in the system resulted in decreases of HONO, NO and NO_2 (60%) formation rates (Figure 6). The O_2^- formation at the surface could explain the formation of nitrate, leading to losses of nitrogen-containing compounds from the gas phase. O_2^- production can result from the formation of peroxy radicals from the surface which were probed in this study (see next section)[66–68]. As O_2^- is formed, the surface becomes more oxidant, potentially leading to an evolution in the mixing ratios of nitrogen containing compounds at the gas-solid interface.

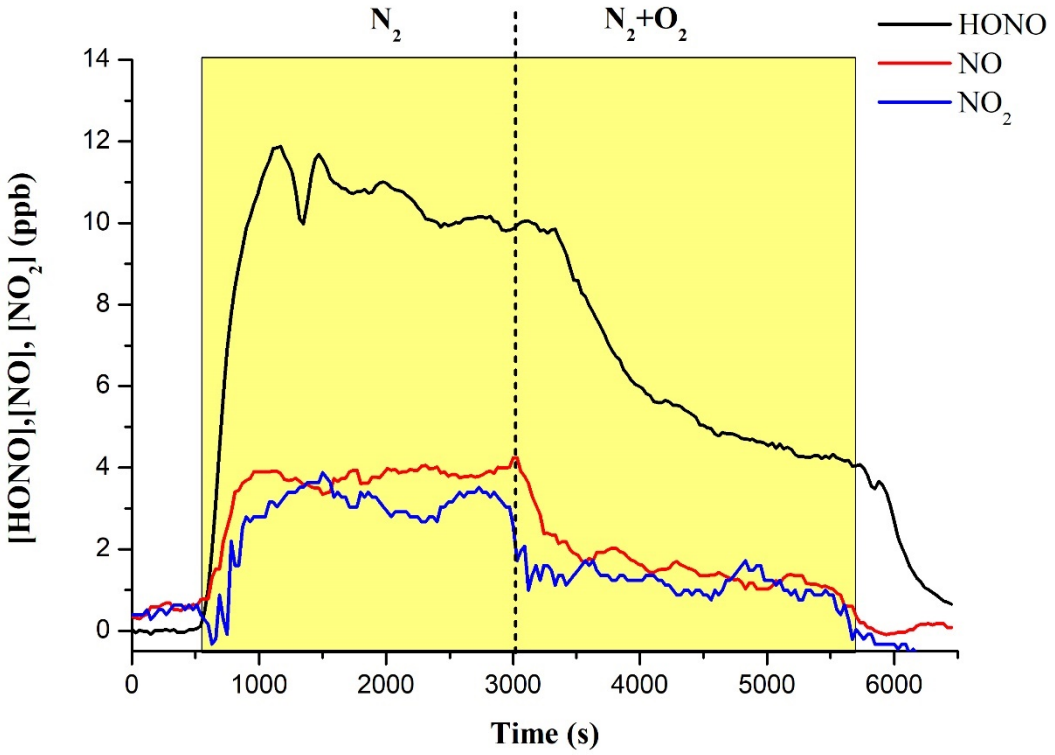

328

329 **Figure 6:** The formation of HONO, NO and NO_2 from a film of furfural + KNO_3 under UV
330 irradiation (yellow section) at RH = 81 ± 2%. The vertical dashed line separates the two
331 conditions: N_2 and N_2 +O_2.

332

333 ***3.4. NO uptake experiments***

334 A typical result for a NO photo-enhanced uptake experiments on irradiated furfural films is
335 presented in Figure 7. The NO was initially chosen as a scavenger of the surface-produced
336 peroxy radicals, similar to the study of Hayeck et al[46]. These radicals can react with NO to
337 produce NO_2 following reaction (R7):

338

$$Sample + h\nu \rightarrow R^{\cdot} \quad \text{(R5)}$$

$$R^{\cdot} + O_2 \rightarrow RO - O^{\cdot} \quad \text{(R6)}$$

$$RO - O^{\cdot} + NO \rightarrow RO^{\cdot} + NO_2 \quad \text{(R7)}$$

339

Tests performed in the absence of O_2 and UV light did not result in any NO uptake due to the absence of peroxy radicals. Under high relative humidity (RH = 81 ± 2%), furfural films were unable to uptake NO. This observation could be linked to the presence of a thin layer of water on the surface of the film, which formed under high relative humidity[39,70]. NO is insoluble in water[71] so no interaction between the surface and NO was observed. Peroxy radicals could also be trapped in the liquid phase, preventing their release in the gas phase to react with NO. However, under indoor-relevant relative humidity (RH = 45 ± 2%), NO is mostly converted into HONO with a yield lower than 30%. It should be noted that the NO_y-mass balance is not closed. That can be explained by the surface formation of nitrogen-containing products.

The radical formation from the surfaces could occur due to the presence of furanone / butenedial under irradiation at $\lambda \geq 235$ nm, 2(5H)-furanone forms an aldehyde-ketene through a ring-opening mechanism[50]. Butenedial is able to form radicals under irradiation[51]. Radicals could also come from the formation of H-abstracted furan and furfural, which were detected in the PTR-TOF-MS analyses.

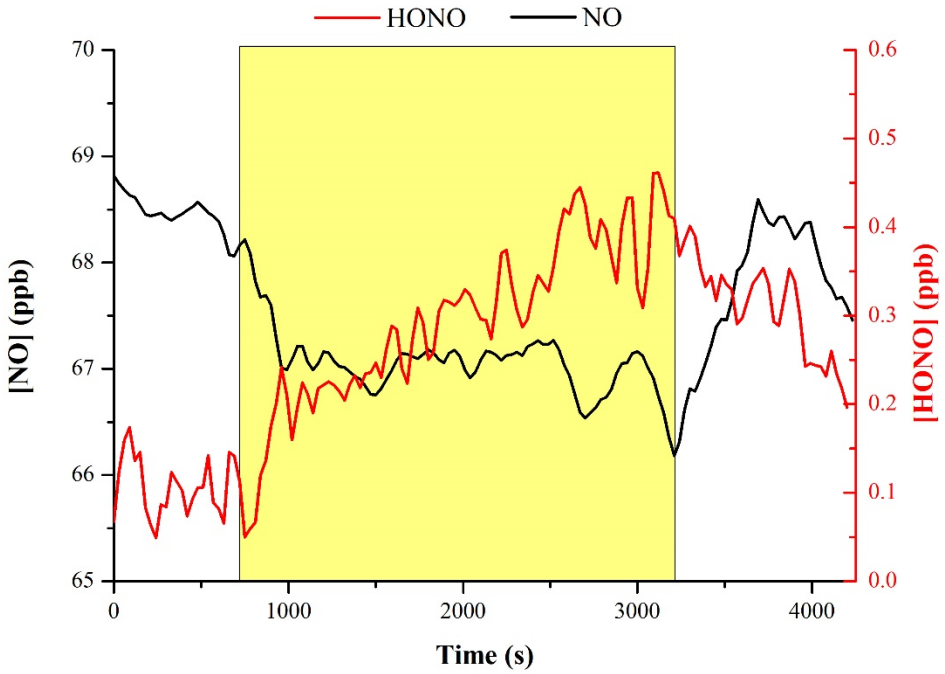

355

356 **Figure 7:** NO uptake and HONO formation from a furfural film (prepared from 2 mL of 0.5
357 M of furfural solution) at RH = 45 ± 2%. Yellow section corresponds to UV irradiation

358

359 ***3.5. Influence of relative humidity***

360 The relative humidity effect on the gas-phase formation of HONO from mixed furfural and
361 nitrate anions films is shown in Figure 8. The maximum relative humidity was below the
362 deliquescence of potassium nitrate (>92%)[73].

363 During the transition from low to high relative humidity, the HONO formation increased due
364 to nitrate photolysis [55]. However, pure potassium nitrate films were unable to produce nitrate.
365 This result could imply that there was a photosensitizer effect from the organic film, which
366 enabled nitrate photochemistry at the surface.

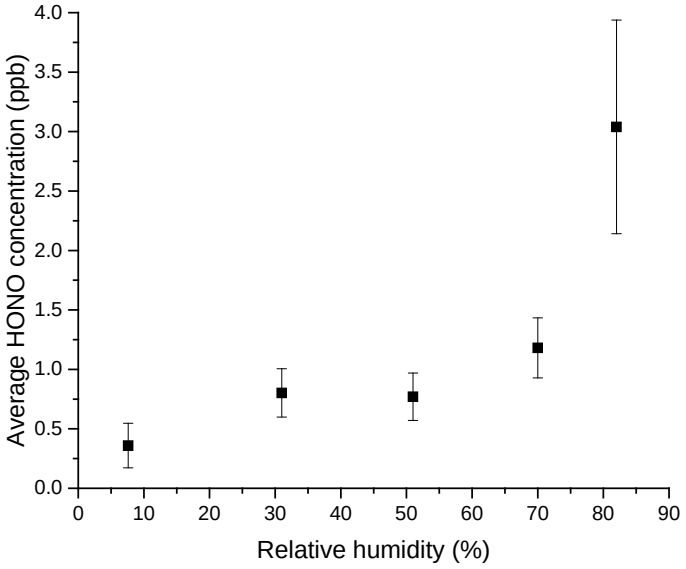

Figure 8: The concentration of HONO formed as a function of relative humidity (%) from a film prepared with 0.1 M KNO_3 and 0.1 M Furfural. Irradiation time = 45 min.

3.6. HONO source indoor

To estimate the concentration of HONO emitted from a surface in a simulated room, HONO emission fluxes (E_{HONO}) in µg m^{-2} h^{-1} were calculated according to Potard[52]:

$$E_{\mathrm{HONO}} = \frac{F_{air} \times ([HONO]_{\mathrm{films}} - [HONO]_{\mathrm{blank}}) \times M_{\mathrm{HONO}}}{V_{\mathrm{mol}}^{\mathrm{air}} \times S_{\mathrm{exposed}}} \qquad \textbf{(Eq. 1)}$$

where F_{air} is the airflow (F_{air} =0.0054 m^3 h^{-1}), $[HONO]_{films}$ and $[HONO]_{blank}$ are the concentrations of HONO emitted from coated samples and clean glass support (ppb), respectively, M_{HONO} is the molecular mass of HONO (0.047 kg mol^{-1}), V_{mol}^{air} is the air molar volume at standard temperature and pressure (25 L mol^{-1} at 25°C and 1 atm) and $S_{exposed}$ is the exposed surface of nitrate and furfural to light (0.002 m^2).

HONO indoor level depends on the production rate, the surface-area-to-volume ratio of the room, the photolysis rate and the ventilation rate. Thus, the indoor concentration of HONO

382 can be determined according to Willem et al.[75]:

$$\frac{d[HONO]}{dt} = \frac{E_{HONO} \times S}{V} - N_h[HONO] - J_{HONO}[HONO] \quad \textbf{(Eq. 2)}$$

383

384 where E_{HONO} is the emission rate of HONO in µg m^{-2} h^{-1}, S is the surface area of the
385 room (m^2), V is the room volume (m^3), N_h is the air exchange rate (h^{-1}) and J_{HONO} is the
386 photolysis rate of indoor HONO. Loss on surfaces was not taken into account here as the reactor
387 used in these experiments present a similar surface-to-volume ratio as the one used in this
388 simulation. Hence, HONO measured is already impacted by the loss on the surfaces.

389 Assuming there is no influence of outdoor concentration of HONO on the indoor
390 concentration due to relatively low outdoor levels[76], the steady-state HONO concentration can
391 be simplified as:

$$[HONO] = \frac{E_{HONO} \times S}{V \times (J_{HONO} + N_h)} \quad \textbf{(Eq. 3)}$$

392

393 For indoor-relevant relative humidity (RH = 45%), with an air exchange rate of 0.5 h^{-1}
394 and a photolysis rate of HONO equal to 0.25 h^{-1} [31,32] and considering the surface of a room of
395 50 m^3 and 94 m^2 is covered from a film obtained from a solution of 0.1 M KNO_3 and 0.1 M
396 Furfural, HONO concentrations are 3.9 ppb.

397 Previous studies were performed on the emission of HONO from the uptake of NO_2 on
398 photocatalytic painted surfaces [28,77,78] and with various household surfaces[23]. Conversion yields
399 up to 90% were observed leading to steady state concentrations of HONO ranging from 1.6 to
400 6.3 ppb. This indicates that furfural film could lead to an increase in HONO production in
401 presence of NO_2.

402 Typical indoor levels of HONO range from 1 to 10 ppb[33,79,80]; as such, indoor HONO

levels could be significantly affected by surface chemistry as it was previously suggested[11,80]. HONO can react with indoor pollutants to form carcinogens like nitrosamines[81] and produce hydroxyl radicals by photolysis. While the direct effect of hydroxyl radicals on health is still uncertain[82,83], its role in the formation of toxic compounds like ozone or aerosols indicates a potential negative effect on indoor air quality.

4. Conclusions

Furfural has been identified as an indoor pollutant[9,15]. Here, we show that this molecule can react on surfaces, producing complex adsorbed products that initiate photochemistry indoors. It especially leads to the formation of VOCs and the humidity-dependent formation of nitrous acid in the presence of co-adsorbed nitrate anions. O_2 can also form peroxy radicals leading to organic nitrate formation on the surface. As wood-based furniture at home is ubiquitous, surfaces coated with furfural oligomer are to be expected. Extrapolation of our results to an indoor environment lead to an estimation of 3.9 ppb at indoor-relevant relative humidity of 45%. HONO reacts with indoor pollutants to form carcinogens compounds as well as producing OH radicals through photolysis. The presence of indoor OH radicals leads to the formation of irritating and toxic compounds, altering the indoor air quality.

Acknowledgments

This work was supported by the Alfred P. Sloan Foundation under its Chemistry of Indoor Environments program.

Data Availability Statement

The data that support the findings of this study are available from the corresponding author upon reasonable request.

References

1. Morrison G. Recent Advances in Indoor Chemistry. *Curr Sustainable Renewable Energy Rep*. 2015;2:33–40.

2. Gao P, Korley F, Martin J, Chen BT. Determination of Unique Microbial Volatile Organic Compounds Produced by Five Aspergillus Species Commonly Found in Problem Buildings. *AIHA Journal*. 2002;63:135–140.

3. Uhde E, Salthammer T. Impact of reaction products from building materials and furnishings on indoor air quality — A review of recent advances in indoor chemistry. In: ; 2007.

4. Brown SK, Sim MR, Abramson MJ, Gray CN. Concentrations of Volatile Organic Compounds in Indoor Air – A Review. *Indoor Air*. 1994;4:123–134.

5. Edwards RD. VOC source identification from personal and residential indoor, outdoor and workplace microenvironment samples in EXPOLIS-Helsinki, Finland. *Atmospheric Environment*. 2001;35:4829–4841.

6. Carslaw N. A new detailed chemical model for indoor air pollution. *Atmospheric Environment*. 2007;41:1164–1179.

7. Waring MS, Wells JR. Volatile organic compound conversion by ozone, hydroxyl radicals, and nitrate radicals in residential indoor air: Magnitudes and impacts of oxidant sources. *Atmospheric Environment*. 2015;106:382–391.

8. Yrieix C, Maupetit F, Ramalho O. Determination of VOC emissions from French wood products. In: *4th European Wood-Based Panel Symposium*. Hanover, Germany; 2004:10 p. September 2004. https://hal.archives-ouvertes.fr/hal-00688527. Accessed July 15, 2019.

9. Cincinelli A, Martellini T, Amore A, et al. Measurement of volatile organic compounds (VOCs) in libraries and archives in Florence (Italy). *Science of The Total Environment*. 2016;572:333–339.

10. Mathew AK, Abraham A, Mallapureddy KK, Sukumaran RK. Lignocellulosic Biorefinery Wastes, or Resources? In: *Waste Biorefinery*. Elsevier; 2018:267–297. 2018. https://linkinghub.elsevier.com/retrieve/pii/B9780444639929000094. Accessed January 8, 2020.

11. Wang C, Collins DB, Arata C, et al. Surface reservoirs dominate dynamic gas-surface partitioning of many indoor air constituents. *Science Advances*. 2020;6:eaay8973.

12. Shin S-H, Jo W-K. Longitudinal variations in indoor VOC concentrations after moving into new apartments and indoor source characterization. *Environ Sci Pollut Res*. 2013;20:3696–3707.

13. Salonen HJ, Pasanen A-L, Lappalainen SK, et al. Airborne Concentrations of Volatile Organic Compounds, Formaldehyde and Ammonia in Finnish Office Buildings with Suspected Indoor Air Problems. *Journal of Occupational and Environmental Hygiene*. 2009;6:200–209.

14. Martellini T, Berlangieri C, Dei L, et al. Indoor levels of volatile organic compounds at Florentine museum environments in Italy. *Indoor Air*. 2020;n/a. February 23, 2020. https://onlinelibrary.wiley.com/doi/abs/10.1111/ina.12659. Accessed July 3, 2020.

15. Nilsson A, Lagesson V, Bornehag C-G, Sundell J, Tagesson C. Quantitative determination of volatile organic compounds in indoor dust using gas chromatography-UV spectrometry. *Environment International*. 2005;31:1141–1148.

16. Zhang J, Chen W, Li J, Yu S, Zhao W. VOCs and Particulate Pollution due to Incense Burning in Temples, China. *Procedia Engineering*. 2015;121:992–1000.

17. Hoydonckx HE, Rhijn WMV, Rhijn WV, Vos DED, Jacobs PA. Furfural and Derivatives. In: *Ullmann's Encyclopedia of Industrial Chemistry*. American Cancer Society; 2007. 2007. https://onlinelibrary.wiley.com/doi/abs/10.1002/14356007.a12_119.pub2. Accessed January 6, 2020.

18. Mariscal R, Maireles-Torres P, Ojeda M, Sádaba I, Granados ML. Furfural: a renewable and versatile platform molecule for the synthesis of chemicals and fuels. *Energy Environ Sci*. 2016;9:1144–1189.

19. Nagda NL. *Design and Protocol for Monitoring Indoor Air Quality*. ASTM International; 1989.

20. Liu Q-T, Chen R, McCarry BE, Diamond ML, Bahavar B. Characterization of Polar Organic Compounds in the Organic Film on Indoor and Outdoor Glass Windows. *Environ Sci Technol*. 2003;37:2340–2349.

21. Weschler CJ, Nazaroff WW. Growth of organic films on indoor surfaces. *Indoor Air*. 2017;27:1101–1112.

22. Kruza M, Lewis AC, Morrison GC, Carslaw N. Impact of surface ozone interactions on indoor air chemistry: A modeling study. *Indoor Air*. 2017;27:1001–1011.

23. Gómez Alvarez E, Sörgel M, Gligorovski S, et al. Light-induced nitrous acid (HONO) production from NO2 heterogeneous reactions on household chemicals. *Atmospheric Environment*. 2014;95:391–399.

24. Sleiman M, Gundel LA, Pankow JF, Jacob P, Singer BC, Destaillats H. Formation of carcinogens indoors by surface-mediated reactions of nicotine with nitrous acid, leading to potential thirdhand smoke hazards. *Proceedings of the National Academy of Sciences*. 2010;107:6576–6581.

25. Ye C, Zhang N, Gao H, Zhou X. Matrix effect on surface-catalyzed photolysis of nitric acid. *Scientific Reports*. 2019;9. December 2019. http://www.nature.com/articles/s41598-018-37973-x. Accessed July 20, 2020.

26. Salthammer T, Bednarek M, Fuhrmann F, Funaki R, Tanabe S-I. Formation of organic indoor air pollutants by UV-curing chemistry. *Journal of Photochemistry and Photobiology A: Chemistry*. 2002;152:1–9.

27. Schwartz-Narbonne H, Jones SH, Donaldson DJ. Indoor Lighting Releases Gas Phase Nitrogen Oxides from Indoor Painted Surfaces. *Environ Sci Technol Lett*. January 2019. January 15, 2019. https://doi.org/10.1021/acs.estlett.8b00685. Accessed January 22, 2019.

28. Bartolomei V, Sörgel M, Gligorovski S, et al. Formation of indoor nitrous acid (HONO) by light-induced NO2 heterogeneous reactions with white wall paint. *Environ Sci Pollut Res*. 2014;21:9259–9269.

29. Gandolfo A, Marque S, Temime-Roussel B, et al. Unexpectedly High Levels of Organic Compounds Released by Indoor Photocatalytic Paints. *Environ Sci Technol*. 2018;52:11328–11337.

30. Gandolfo A, Gligorovski V, Bartolomei V, et al. Spectrally resolved actinic flux and photolysis frequencies of key species within an indoor environment. *Building and Environment*. 2016;109:50–57.

31. Alvarez EG, Amedro D, Afif C, et al. Unexpectedly high indoor hydroxyl radical concentrations associated with nitrous acid. *PNAS*. 2013;110:13294–13299.

32. Zhou S, Young CJ, VandenBoer TC, Kowal SF, Kahan TF. Time-Resolved Measurements of Nitric Oxide, Nitrogen Dioxide, and Nitrous Acid in an Occupied New York Home. *Environ Sci Technol*. 2018;52:8355–8364.

33. Gligorovski S. Nitrous acid (HONO): An emerging indoor pollutant. *Journal of Photochemistry and Photobiology A: Chemistry*. 2016;314:1–5.

34. Gómez Alvarez E, Wortham H, Strekowski R, Zetzsch C, Gligorovski S. Atmospheric Photosensitized Heterogeneous and Multiphase Reactions: From Outdoors to Indoors. *Environ Sci Technol*. 2012;46:1955–1963.

35. Gligorovski S, Weschler CJ. The Oxidative Capacity of Indoor Atmospheres. *Environ Sci Technol*. 2013;47:13905–13906.

36. Mendez M, Amedro D, Blond N, et al. Identification of the major HOx radical pathways in an indoor air environment. *Indoor Air*. 2017;27:434–442.

37. Weschler CJ, Shields HC, Naik DV. Indoor Chemistry Involving O3, NO, and NO2 as Evidenced by 14 Months of Measurements at a Site in Southern California. *Environmental Science & Technology*. 1994;28:2120–2132.

38. Arata C, Zarzana KJ, Misztal PK, et al. Measurement of NO3 and N2O5 in a Residential Kitchen. *Environ Sci Technol Lett*. 2018;5:595–599.

39. Schwartz-Narbonne H, Donaldson DJ. Water uptake by indoor surface films. *Scientific Reports*. 2019;9:1–10.

40. Baergen AM, Donaldson DJ. Seasonality of the Water-Soluble Inorganic Ion Composition and Water Uptake Behavior of Urban Grime. *Environ Sci Technol*. 2019;53:5671–5677.

41. Ponczek M, George C. Kinetics and Product Formation during the Photooxidation of Butanol on Atmospheric Mineral Dust. *Environ Sci Technol*. 2018;52:5191–5198.

42. Ŝpaněl P, Ji Y, Smith D. SIFT studies of the reactions of H3O+, NO+ and O2+ with a series of aldehydes and ketones - ScienceDirect. 1997. https://www-sciencedirect-com.docelec.univ-lyon1.fr/science/article/pii/S0168117697001663?via%3Dihub. Accessed November 27, 2019.

43. Heland J, Kleffmann J, Kurtenbach R, Wiesen P. A New Instrument To Measure Gaseous Nitrous Acid (HONO) in the Atmosphere. *Environ Sci Technol*. 2001;35:3207–3212.

44. Gandini A, Belgacem MN. Furans in polymer chemistry. *Progress in Polymer Science*. 1997;22:1203–1379.

45. van Zandvoort I, Wang Y, Rasrendra CB, et al. Formation, Molecular Structure, and Morphology of Humins in Biomass Conversion: Influence of Feedstock and Processing Conditions. *ChemSusChem*. 2013;6:1745–1758.

46. Shi N, Liu Q, Ju R, et al. Condensation of α-Carbonyl Aldehydes Leads to the Formation of Solid Humins during the Hydrothermal Degradation of Carbohydrates. *ACS Omega*. 2019;4:7330–7343.

47. Sumerskii IV, Krutov SM, Zarubin MY. Humin-like substances formed under the conditions of industrial hydrolysis of wood. *Russ J Appl Chem*. 2010;83:320–327.

48. Filiciotto L, Miguel G de, Balu AM, Romero AA, Waal JC van der, Luque R. Towards the photophysical studies of humin by-products. *Chem Commun*. 2017;53:7015–7017.

49. Bovey FA, Mirau PA. *NMR of Polymers*. Academic Press; 1996.

50. Li X, Lan X, Wang T. Highly selective catalytic conversion of furfural to γ-butyrolactone. *Green Chem*. 2016;18:638–642.

51. Newland MJ, Rea GJ, Thüner LP, et al. Photochemistry of 2-butenedial and 4-oxo-2-pentenal under atmospheric boundary layer conditions. *Phys Chem Chem Phys*. 2019;21:1160–1171.

52. Breda S, Reva I, Fausto R. UV-induced unimolecular photochemistry of 2(5H)-furanone and 2(5H)-thiophenone isolated in low temperature inert matrices. *Vibrational Spectroscopy*. 2009;50:57–67.

53. Smets G. Organic Polymer Photochemistry. *Polymer Journal*. 1985;17:153–165.

54. Ye C, Zhang N, Gao H, Zhou X. Matrix effect on surface-catalyzed photolysis of nitric acid. *Scientific Reports*. 2019;9:1–10.

55. Zhou X, Gao H, He Y, et al. Nitric acid photolysis on surfaces in low-NOx environments: Significant atmospheric implications. *Geophysical Research Letters*. 2003;30. December 1, 2003. https://agupubs-onlinelibrary-wiley-com.docelec.univ-lyon1.fr/doi/abs/10.1029/2003GL018620. Accessed December 5, 2018.

56. Bravo M, Olwiert AC, Oelckers B. Nitrate determination in Chilean Caliche samples by UV-Visble absorbance measurements and multivariate calibraron. *Journal of the Chilean Chemical Society*. 2009;54:93–98.

57. Sager EE, Byers FC. Spectral absorbance of some aqueous solutions in the range 10-degrees to 40-degrees-C. *Journal of Research of the National Bureau of Standards.* 1957;58:33.

58. Yang W, Han C, Yang H, Xue X. Significant HONO formation by the photolysis of nitrates in the presence of humic acids. *Environmental Pollution*. 2018;243:679–686.

59. Chapman OL, Heckert DC, Reasoner JW, Thackaberry SP. Photochemical Studies on 9-Nitroanthracene1. *J Am Chem Soc*. 1966;88:5550–5554.

60. Feilberg A. Atmospheric Chemistry of Polycyclic Aromatic Compounds with Special Emphasis on Nitro Derivatives. January 2020.

61. Ramazan KA, Syomin D, Finlayson-Pitts BJ. The photochemical production of HONO during the heterogeneous hydrolysis of NO2. *Phys Chem Chem Phys*. 2004;6:3836–3843.

62. Saliba NA, Mochida M, Finlayson-Pitts BJ. Laboratory studies of sources of HONO in polluted urban atmospheres. *Geophysical Research Letters*. 2000;27:3229–3232.

63. Gutzwiller L, Arens F, Baltensperger U, Gäggeler HW, Ammann M. Significance of Semivolatile Diesel Exhaust Organics for Secondary HONO Formation. *Environ Sci Technol*. 2002;36:677–682.

64. Stemmler K, Ndour M, Elshorbany Y, et al. Light induced conversion of nitrogen dioxide into nitrous acid on submicron humic acid aerosol. *Atmos Chem Phys*. 2007:12.

65. Wall KJ, Harris GW. Uptake of nitrogen dioxide (NO2) on acidic aqueous humic acid (HA) solutions as a missing daytime nitrous acid (HONO) surface source. *J Atmos Chem*. 2017;74:283–321.

66. Sonntag C von, Schuchmann H-P. The Elucidation of Peroxyl Radical Reactions in Aqueous Solution with the Help of Radiation-Chemical Methods. *Angewandte Chemie International Edition in English*. 1991;30:1229–1253.

67. Tan Y, Lim YB, Altieri KE, Seitzinger SP, Turpin BJ. Mechanisms leading to oligomers and SOA through aqueous photooxidation: insights from OH radical oxidation of acetic acid and methylglyoxal. *Atmospheric Chemistry and Physics*. 2012;12:801–813.

68. Schuchmann MN, Zegota H, Sonntag C von. Acetate Peroxyl Radicals, ·O2CH2 CO2-: A Study on the γ-Radiolysis and Pulse Radiolysis of Acetate in Oxygenated Aqueous Solutions. *Zeitschrift für Naturforschung B*. 1985;40:215–221.

69. Hayeck N, Rossignol S, Alpert PA, et al. Photochemical reaction at the air-water interface and effect on atmospheric nitric oxide. In: *European Aerosol Conference, EAC 2016*. Tours , France; 2016. September 2016. https://hal.archives-ouvertes.fr/hal-01364534. Accessed March 10, 2020.

70. Dubowski Y, Sumner AL, Menke EJ, et al. Interactions of gaseous nitric acid with surfaces of environmental interest. *Phys Chem Chem Phys*. 2004;6:3879–3888.

71. Zacharia IG, Deen WM. Diffusivity and solubility of nitric oxide in water and saline. *Ann Biomed Eng*. 2005;33:214–222.

72. Breda S, Reva I, Fausto R. UV-induced unimolecular photochemistry of 2(5H)-furanone and 2(5H)-thiophenone isolated in low temperature inert matrices. *Vibrational Spectroscopy*. 2009;50:57–67.

73. Freney EJ, Martin ST, Buseck PR. Deliquescence and Efflorescence of Potassium Salts Relevant to Biomass-Burning Aerosol Particles. *Aerosol Science and Technology*. 2009;43:799–807.

74. Potard K. Les émissions de composés organiques volatiles (COVs) des sols dans les paysages agricoles: identification des sources et incidences sur la qualité de l'air. :182.

75. Willem H, Hult E, Hotchi T, Russell M, Maddalena R, Singer B. Ventilation Control of Volatile Organic Compounds in New U.S. Homes: Results of a Controlled Field Study in Nine Residential Units.

76. Lee Kiyoung, Xue Jianping, Geyh Alison S, et al. Nitrous acid, nitrogen dioxide, and ozone concentrations in residential environments. *Environmental Health Perspectives*. 2002;110:145–150.

77. Gandolfo A, Bartolomei V, Gomez Alvarez E, et al. The effectiveness of indoor photocatalytic paints on NOx and HONO levels. *Applied Catalysis B: Environmental*. 2015;166–167:84–90.

78. Gandolfo A, Bartolomei V, Truffier-Boutry D, et al. The impact of photocatalytic paint porosity on indoor NOx and HONO levels. *Phys Chem Chem Phys*. 2020;22:589–598.

79. Leaderer BP, Naeher L, Jankun T, et al. Indoor, outdoor, and regional summer and winter concentrations of PM10, PM2.5, SO4(2)-, H+, NH4+, NO3-, NH3, and nitrous acid in homes with and without kerosene space heaters. *Environ Health Perspect*. 1999;107:223–231.

80. Collins DB, Hems RF, Zhou S, et al. Evidence for Gas–Surface Equilibrium Control of Indoor Nitrous Acid. *Environ Sci Technol*. 2018;52:12419–12427.

81. Sleiman M, Destaillats H, Smith JD, et al. Secondary organic aerosol formation from ozone-initiated reactions with nicotine and secondhand tobacco smoke. *Atmospheric Environment*. 2010;44:4191–4198.

82. Gligorovski S, Wortham H, Kleffmann J. The hydroxyl radical (OH) in indoor air: Sources and implications. *Atmospheric Environment*. 2014;99:568–570.

83. Weschler CJ, Wells JR, Poppendieck D, Hubbard H, Pearce TA. Workgroup Report: Indoor Chemistry and Health. *Environ Health Perspect*. 2006;114:442–446.